STUDY OF THE PARABOLIC AND ELLIPTIC APPROACHES VALIDITIES FOR A TURBULENT CO-FLOWING JET

Houda MAHMOUD[1*], Wassim KRIAA[1], Hatem MHIRI[1], Georges Le PALEC[2], Philippe BOURNOT[2]

[1] Unité de thermique et thermodynamique des procédés industriels, Ecole Nationale d'Ingénieurs de Monastir, route de Ouardanine, 5000 MONASTIR, TUNISIE

[2] IUSTI, UMR CNRS 6595, 5 Rue Enrico Fermi, Technopôle de Château- Gombert, 13013 Marseille, France

[*] Corresponding author; e-mail: *mahhouda2003@yahoo.fr

An axisymmetric turbulent jet discharged in a co-flowing stream was studied with the aid of parabolic and elliptic approaches. The simulations were performed with two in-house codes. Detailed comparisons of data show good agreement with the corresponding experiments; and different behaviors of jet dilution were found in initial region at different ranges of velocities ratios. It has been found that the two approaches give practically the same results for the velocities ratios $R_u \leq 1.5$. Further from this value, the elliptic approach highlights the appearance of the fall velocity zone and that's due to the presence of a trough low pressure. This fall velocity has not been detected by the parabolic approach and that's due to the jet entrainment by the ambient flow. The intensity of this entrainment is directly related to the difference between the primary (jet) and the secondary flow (co-flow). In fact, by increasing the velocities ratios R_u, the sucked flux by the outer stream becomes more important; the fall velocity intensifies and changes into a recirculation zone for $R_u \geq 5$.

Key words: *Axisymmetric jet, turbulence, co-flow, recirculation zone, parabolic approach, elliptic approach.*

1. Introduction

The turbulent jets emerged in a moving stream exist widely in nature as well as in propulsion systems, reactors, engines, etc. The ability to predict the turbulent mixing in flows with complex features is vital for modeling the dynamics of such flows and a prerequisite for predicting turbulent combustion situation [1].

In this context, several experimental [2-5] and numerical [6-8] works have been devoted. The experiments on co-flowing jets have been piloted since 1973, with low velocities ratios (R_u ranging between 0.01 and 0.33). The purpose is to solve the seeding problems found at the jet edge and to avoid the oscillations development in the primary flow. Antonia and Bilger [2] were the first who led an experimental study on turbulent jets emerged in a co-flow with velocities ratios ranging between 0.22 and 0.33. These authors have shown that such flow does not reach an asymptotic state. Afterwards, Nickels and Perry [3] proved the existence of the self-similarity zone. They showed that,

for a velocity ratio R_u = *0.09*, the radial profiles of the mean streamwise velocity collapse fairly well far downstream (*x/d*=30*)*. Also, they noted that the flow becomes independent from initial conditions at an axial distance strongly depending on initial momentum. Mesnier [4] investigated three turbulent jets, including helium, air and CO_2 jets exiting with 40 m/s velocity in a low-speed air co-flow. He was concerned to study density and nozzle geometry effects on jet structure. Antoine et al. [5] performed measurements in turbulent water jet flowing with an injection velocity equal to 10 m/s and emerging in a low-speed co-flow water (R_u = 0.05). They showed that co-flow reduces the jet spreading rate by approximately 30% from the free jet.

Numerically, the study of turbulent jets emerging in a co-flow with low velocities ratios has been the subject of several works [6-7] in order to stabilize the calculations and to ensure the codes convergence. These studies, conducted with small velocities ratios ($0.01 \leq R_u \leq 0.2$), are based on the elliptic (complete equations) or parabolic approach (boundary layer assumptions). Imine et al. [6] performed their numerical simulation on an axisymmetric isothermal and turbulent jet discharged in a co-flow at a velocity ratio R_u equal to 0.01. They used the elliptic approach and the second order model (RSM). These authors are interested to study the nozzle geometry and the densities ratios influence on the jet mixing rate and on mean and turbulent flow parameters. They showed that the asymmetric geometry improve the mixing process of the turbulent co-flowing jet. Habli et al. [7] used the parabolic approach, the first and the second order model to study an axisymmetric turbulent jet moving in a co-flow with different velocities ratios (R_u ranging between *0* and *0.2)*. They focused their work on the test of Reynolds Stress algebraic Model (RSM) performance compared to that of the standard $k-\varepsilon$ model in predicting the average and the turbulent flow sizes in free and forced convection modes. Also, they are interested to the influence of the velocities ratios on the jet typical parameters and self-similarity zone. These authors showed that the two considered models give similar results in forced convection mode. In contrast, in free convection mode, the second order model is better than the $k-\varepsilon$ model in modeling buoyancy and turbulence structures.

This bibliographic review shows that all experimental and numerical studies have considered low velocities ratios R_u ranging between 0.01 and 0.33. However, a co-flowing jet with large velocities ratios is a new method of flame stabilization [8] and a desire of many industrial applications. In this context, in our last publication [9] we studied an axisymmetric turbulent jet discharging into co-flowing stream with different velocities ratios ranging between 0 and ∞. The results showed that the two turbulence models: standard k-ε and the RSM (Reynolds Stress Model) are valid to predict the average and turbulent flow sizes. Also, the effect of the velocities ratios on the flow structure was examined. It is noted, for $R_u > 1$, the appearance of a fall velocity zone due to the presence of a trough low pressure. This fall velocity becomes increasingly intense according to R_u and changes into a recirculation zone for $R_u \geq 4.5$.

In this paper, we propose to study the limit of the parabolic approach validity compared to the elliptic one, to predict the turbulent co-flowing jet structure for a large range of velocities ratios (R_u varied between 0 and 10). The resolution of the governing equations was performed by two computer codes: the first code use the elliptic approach (complete equations governing the flow without the boundary layer approximations) while the second code is based on the parabolic approach (equations with boundary layer assumptions).

2. Numerical modeling

2.1. Assumptions

The flow configuration and the associated parameters used in the present study are the same as those used by Mesnier [4] for its measurements (*Fig.1)*. A turbulent jet, with a discharge velocity $U_{0,}$ issues out from a circular nozzle of diameter d equal to *7mm,* in a co-flowing atmosphere of the same fluid which has a velocity U_{∞}. The flow is assumed to be incompressible, axisymmetric and mean steady in nature. The Reynolds number $\mathrm{Re} = u_0 d/\nu$ is assumed large enough for the flow to be fully turbulent at the considered distances from the nozzle. A cylindrical coordinate system may be used, with *x* the axial position, originating from the nozzle, and *r* the radial distance from the nozzle axis.

2.2. Governing equations

Based on the above assumptions and the following dimensionless variables (1), the Reynolds-averaged Navier-Stokes (RANS) equations written in cylindrical coordinates were used by the parabolic and elliptic approaches.

$$X = \frac{x}{d} \quad R = \frac{r}{d} \quad U = \frac{\overline{u}}{\overline{u}_0} \quad V = \frac{\overline{v}}{\overline{u}_0} \quad K = \frac{k}{\overline{u}_0^2} \quad E = \frac{\varepsilon d}{\overline{u}_0^3} \quad P = \frac{p}{\rho \overline{u}_0^2} \tag{1}$$

For the elliptic approach and according to the Reynolds averaged decomposition, the transport equations can be written as follows:

$$\frac{\partial(RU)}{\partial X} + \frac{\partial(RV)}{\partial R} = 0 \tag{2}$$

$$\frac{\partial(UU)}{\partial X} + \frac{1}{R}\frac{\partial(RVU)}{\partial R} = -\frac{\partial P}{\partial X} + \frac{\partial}{\partial X}\left(-\overline{U'U'}\right) + \frac{1}{R}\frac{\partial}{\partial R}\left(-R\overline{U'V'}\right) \tag{3}$$

$$\frac{\partial(UV)}{\partial X} + \frac{1}{R}\frac{\partial(RVV)}{\partial R} = -\frac{\partial P}{\partial R} + \frac{\partial}{\partial X}\left(-\overline{U'V'}\right) + \frac{1}{R}\frac{\partial}{\partial R}\left(-R\overline{V'V'}\right) \tag{4}$$

Taking into account that the two models: standard $k-\varepsilon$ and Reynolds stress model (RSM) predict well the characteristic sizes of the turbulent co-flowing jet [7, 9] and the standard $k-\varepsilon$ model is inexpensive and easy to implement, it will be adopted in this work.

The dimensionless turbulent kinetic energy and dissipation rate equations can be written in the following way:

$$\frac{\partial(UK)}{\partial X} + \frac{1}{R}\frac{\partial}{\partial R}(RVK) = \frac{\partial}{\partial X}\left(\frac{1}{\mathrm{Re}_t\,\sigma_k}\frac{\partial K}{\partial X}\right) + \frac{1}{R}\frac{\partial}{\partial R}\left(\frac{R}{\mathrm{Re}_t\,\sigma_k}\frac{\partial K}{\partial R}\right) + P_k - E \tag{5}$$

$$\frac{\partial(UE)}{\partial X} + \frac{1}{R}\frac{\partial}{\partial R}(RVE) = \frac{\partial}{\partial X}\left(\frac{1}{\mathrm{Re}_t\,\sigma_\varepsilon}\frac{\partial E}{\partial X}\right) + \frac{1}{R}\frac{\partial}{\partial R}\left(\frac{R}{\mathrm{Re}_t\,\sigma_\varepsilon}\frac{\partial E}{\partial R}\right) + C_{\varepsilon 1}\frac{E}{K}P_k - C_{\varepsilon 2}\frac{E^2}{K} \tag{6}$$

P_k is the production term of the turbulent kinetic energy given by the following relation:

$$P_K = \frac{1}{\mathrm{Re}_t}\left(2\left(\left(\frac{\partial U}{\partial X}\right)^2+\left(\frac{\partial V}{\partial R}\right)^2+\left(\frac{V}{R}\right)^2\right)+\left(\left(\frac{\partial U}{\partial X}\right)+\left(\frac{\partial V}{\partial R}\right)\right)^2\right) \quad (7)$$

We note that the Reynolds constraints tensor terms $\overline{U_i' U_j'}$ (i, j = 1 or 2) are modelled by the approximations proposed by Martynenko et al. [10]. The constants numerical values of the standard $k-\varepsilon$ model are given in tab.1 [11].

Tab.1.Empirical constants of the standard $k-\varepsilon$ model [11]

c_μ	c_k	σ_ε	$c_{\varepsilon 1}$	$c_{\varepsilon 2}$	σ_k
0.09	1.0	1.3	1.44	1.92	1

For the parabolic approach, we used the standard $k-\varepsilon$ model by considering the boundary layer approximations. These equations are given by Habli et al. [7].

2.3. Dimensionless boundary conditions

The dimensionless boundary (8) and inlet (9) conditions are written into the following way:
For $X > 0$:

$$\begin{cases} \mathrm{V} = \dfrac{\partial U}{\partial R} = \dfrac{\partial K}{\partial R} = \dfrac{\partial E}{\partial R} = \dfrac{\partial P}{\partial R} = 0 & \text{for} \quad R = 0 \\ \mathrm{U} = R_u, \mathrm{P} = 0, \mathrm{K} = \mathrm{K}_\infty, \mathrm{E} = \mathrm{E}_\infty & \text{for} \quad \mathrm{R} \to \infty \end{cases} \quad (8)$$

In this study, we considered several types of emission conditions. The following system gives the uniforms' velocity profile:
For X=0:

$$\begin{cases} \mathrm{V}=0, U = 1, K = K_0, E = E_0 & \text{for } 0 \le R < 1/2 \\ \mathrm{V}=0, U = R_u, K = K_\infty, E = E_\infty, P = 0 & \text{for } R \ge 1/2 \end{cases} \quad (9)$$

The inlet turbulent kinetic energy k_0 is deduced from the turbulent intensity I (10) given by Mesnier [4], *I = 4.17%.*

$$k_0 = 3/2\left(I.u_0\right)^2 \quad (10)$$

For a jet with an axial symmetry, the inlet dissipation rate of the turbulent kinetic energy is calculated by the following relation [12]:

$$\varepsilon_0 = k_0^{3/2} / l \tag{11}$$

The turbulence length scale l is a physical quantity related to the size of the large eddies that contain the energy in turbulent flows. In the axisymmetric jet, l is restricted by the half of the nozzle diameter.

The turbulent kinetic energy K_∞ and the dissipation rate E_∞ at the co-flow emission are calculated by the following correlations [13]:

$$k_\infty = 3/2\left(u_\infty I\right)^2 \tag{12}$$

$$\varepsilon_\infty = C_\mu^{3/4}.k_\infty^{3/2} / 0.07.l \tag{13}$$

The experimental emission profiles of Mesnier [4] and Antoine et al. [5] were used to study the validity of the elaborated codes with velocities ratios R_u respectively equal to 0.01 and 0.05.

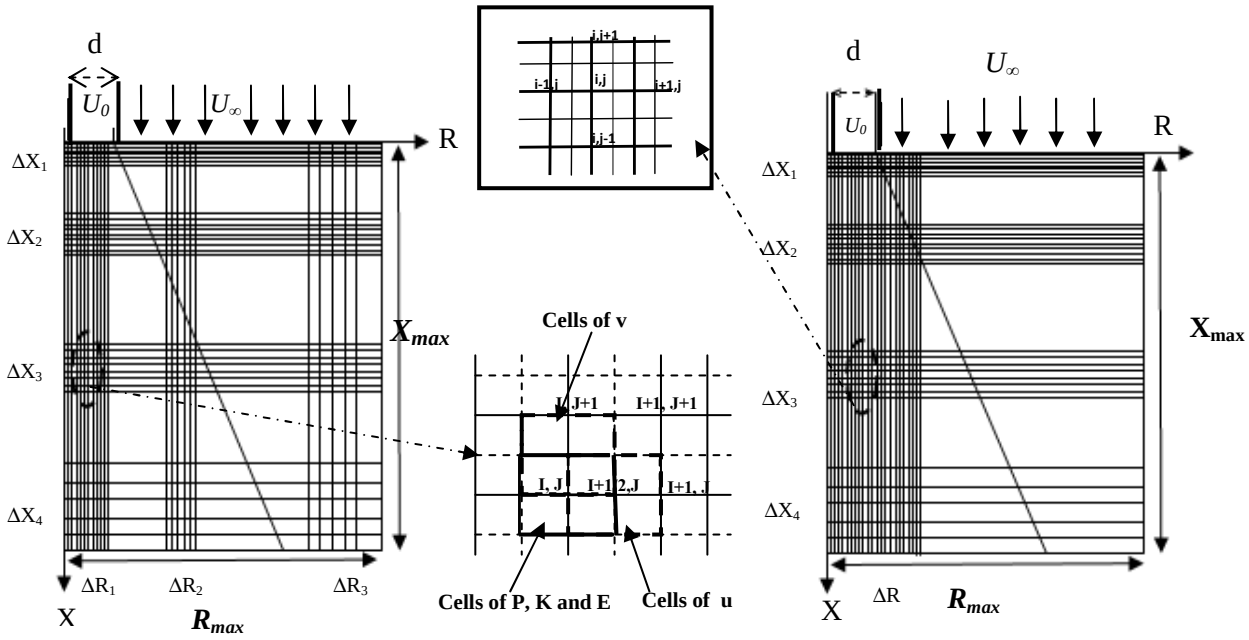

Fig.1a. Grid of the elliptic approach **Fig.1b. Grid of the parabolic approach**

Fig.1. Grid and domain of the studied configuration

2.4. Numerical method

The numerical resolution of the elliptic approach equations (2-6) associated to their boundary and emission conditions (8-9) was carried out by an in-house code based on a finite volume method and a SIMPLE algorithm resolution. The transport equations were discretized using a hybrid scheme

and a staggered grid. This method was adopted for numerical stability reasons. The idea is to evaluate scalar variables, such as pressure, at ordinary nodal points but to calculate velocity components on staggered grids centred on the cell faces (*Fig. 1a*). In fact, the axial velocity cell is centred at the nodes (i + 1/2, j), the radial component cell at the nodes (i, j + 1/2), whereas the pressure term, the kinetic energy and the dissipation rate are centred at the nodes (i, j).

For all the treated cases, the investigation domain dimensions according to X and R depend on the injection velocities ratios R_u ($50 \leq X \leq 160$ and $30 \leq R \leq 60$). Indeed, the domain is very undersized when the velocity is extremely high.

In the longitudinal and transverse directions, the used grid is not uniform. Indeed, the step was taken very small in the nozzle vicinity ($\Delta X \approx \Delta R \approx 10^{-2}$). A little further, the step of calculation increased ($\Delta X \approx \Delta R \approx 10^{-1}$) (*Fig.1a*).

To improve the accuracy of the numerical results for the elliptic approach, we conducted a series of grid independency tests for each set velocity ratio. For R_u = 0.01, we applied the test for three additional grids: 1- a coarse mesh with 504×277 nodes; 2- a medium mesh with 504×427 nodes; and 3- a more refinement mesh with 558×427 nodes. We can observe in Fig.2a that the passage through the grid refinement from the coarse grid to the medium grid caused big difference in the predicted relative pressure. However, the calculations using the fine mesh (558×427) gives similar results as using the medium grid (504×427). Thus, we presumed that the results obtained on the (504×427) mesh do not depend on the grid. Therefore, we conducted all the simulations with the medium grid 504×427.

For the parabolic approach, the numerical resolution of the system equations was carried out using another in-house code based on a finite difference method with a shifted grid. In fact, the transport equations of momentum, energy, turbulent kinetic energy and its dissipation were discretized at the nodes (i + 1/2, j), whereas the continuity equation was discretized at the nodes (i + 1/ 2, j + 1/2). The obtained discretized equations are then solved by adopting a non linear Gauss Seidel method [11] used in a former work [12]. This method was adopted for numerical stability reasons as compared to a non-shifted grid method.

In the longitudinal direction, the used grid is not uniform. In this direction, we tested different steps (Fig.2b). Then, we showed that taking ΔX1=0.001 for X<5 and ΔX2=0.01 for X>5 is sufficient to obtain a numerical solution independent of the grid. In the transverse direction, the used grid is uniform and the calculation step was constant ($\Delta R = 10^{-2}$). Its value imposed a sufficient number of points in this direction, so that the jet was not cut.

For the two approaches, the obtained equations were solved line by line using the algorithm TDMA (Tri-Diagonal Matrix Algorithm). The convergence of the calculations was obtained when the sum of normalized residues was less than 10^{-5}.

For the two approaches, the obtained equations were solved line by line using the algorithm TDMA (Tri-Diagonal Matrix Algorithm). The convergence of the calculations was obtained when the sum of normalized residues was less than 10^{-5}. In fact, when the discretized equation is written in the following way: $a_p \phi_p = \sum a_{nb} \phi_{nb} + S_\phi$, the normalized residue is the difference between the two terms of this equation divided by $\sum_p \left| a_p \phi_p \right|$:

$$R_n = \frac{\sum_{noeudP} \left| \sum_{nb} a_{nb} \phi_{nb} + S_\phi - a_p \phi_p \right|}{\sum_p \left| a_p \phi_p \right|}$$

(ϕ_p is the variable U, V, K or E in the node; a_{nb} and a_p are the coefficients of the discretized equation and S_ϕ is the source term of this equation).

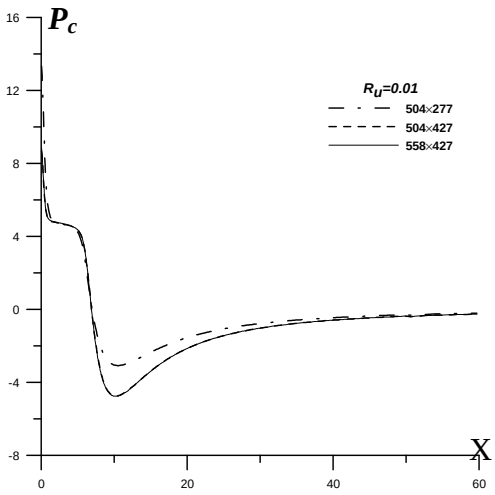

Fig. 2a. Effect of the grid on the centerline relative pressure (Elliptic approach)

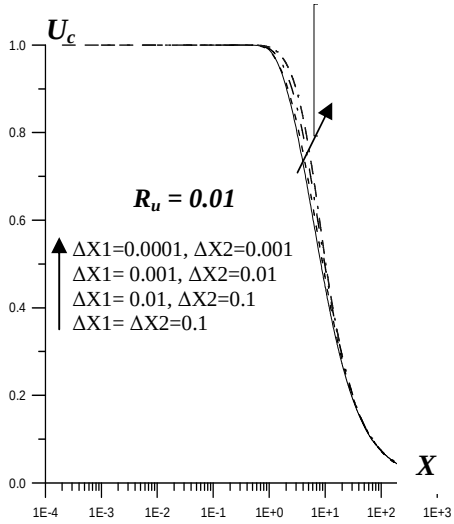

Fig. 2b. Effect of the grid on the centerline vertical velocity (Parabolic approach)

3. Results and discussion

The first stage of calculation consisted primarily in testing the developed programs based on parabolic and elliptic approaches. To validate our numerical computations, the obtained results are compared with the experimental data of Mesnier [4] and Antoine et al. [5]. Then, we undertook a parametric study of the two approaches ability in depicting the co-flowing stream effects on the behavior of the jet flow.

3.1. COMPARAISON BETWEEN COMPUTATION RESULTS AND EXPERIMENTAL DATA

Two in-house codes were developed in order to study the behavior of the co-flowing jet under large range of velocities ratios. The first code is developed to solve the parabolic approach equations and the second is elaborated to solve the elliptic approach equations. To validate these two codes, the calculated mean quantities were compared to the results of Mesnier [4] proposed in initial and intermediate regions and with the results of Antoine et al. [5] given in the developed zone.

The initial conditions used for the validation with the experimental data of Mesnier [4] correspond to a velocities ratio R_u equal to *0.01* and a Reynolds number equal to 23115. In this case, the calculations started from an axial distance X = 0.3. To compare our numerical simulation with the experimental data of Antoine et al. [5], we used an initial velocities ratio R_u = *0.05*, a fully developed velocity profile at the nozzle exit and a Reynolds number Re=10000.

In Fig.3a, we represented the axial evolution of the normalized centerline vertical velocity in the two first zones. It is noted that, overall, the results of the two codes are very close and satisfactory. In fact, closely to the nozzle $X \leq 2$, the results of the two codes are similar and agree well with the experimental data of Mesnier [4]. For $X > 2$, a small difference, which does not exceed 2% is observed between the results of the two codes. The comparison between the experimental data of Mesnier [4]

and our numerical results showed that, for $2 < X \leq 12$, the elliptic approach results are closer to those experimental. On the other hand, for $X > 12$, the results of the parabolic approach are closest with those of experiment. Nevertheless, the differences between the experimental and numerical results remain acceptable and can be explained by experiment errors [4, 6] quoted in former work.

The streamwise distribution of the centreline vertical excess velocity U_{exc} (Antoine et al. [5] configuration) is presented in Fig.3b. It illustrates a satisfactory agreement between the results of the two computer codes in the different flow regions. By comparing the numerical results with those experimental of Antoine et al. [5], we note that, starting from an axial distance $X = 50$, the results are in perfect agreement.

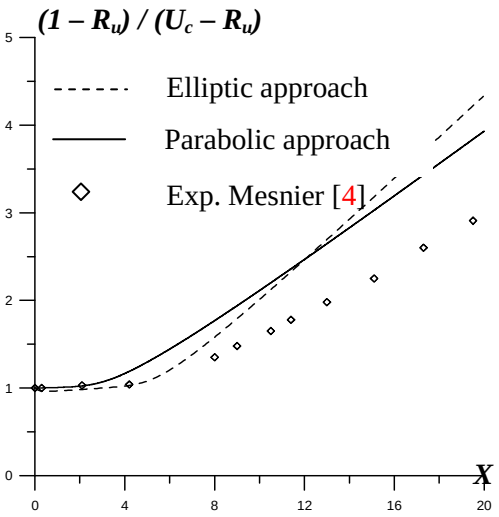

Fig.3a. Axial evolution of the normalized reverse centerline vertical velocity

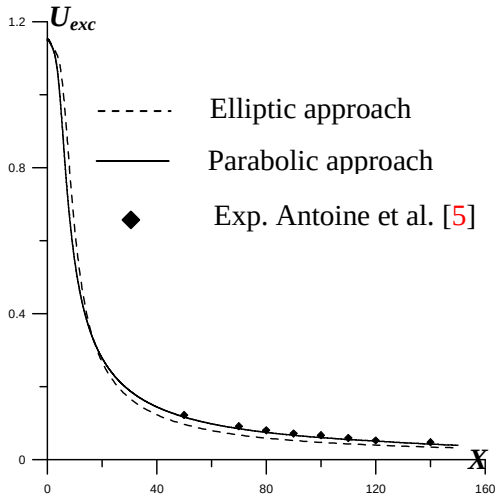

Fig.3b. Axial evolution of the centerline vertical excess velocity

Based on Mesnier [4] configuration, the radial evolution of the normalized vertical velocity is given in fig.4 for the different axial sections: near from the nozzle ($X = 0.3$) and far downstream ($X = 10$ and $X = 20$). It is noted that the results of the two codes are very close whatever the axial section. Facing these statistics to those experimental of Mesnier [4], it is shown that for $X = 0.3$ (Fig.4a), the numerical and experimental results agree well and overall the results of the elliptic approach are closer to the experiment. Further (Fig.4b), the simulation data are in close agreement with those proposed by Mesnier [4] for radial distances $R \geq 1$, i.e. far from the jet axis. For $R<1$, the two codes underestimate the normalized vertical velocity from approximately 15%.

The axial evolution of the normalized centerline turbulent kinetic energy is shown in fig.5a in the jet and transition regions. It is noted that overall the results of the two codes are very close to the experiment [4]. Indeed, the results of the elliptic approach are in good agreement with the experimental data of Mesnier [4] in the vicinity ($X \leq 5$) and far from the nozzle ($X \geq 14$). For the parabolic approach the results are close to the experiment and are considered to be acceptable. For $5 < X < 14$, the two codes overestimate the normalized centerline turbulent kinetic energy maximum. In this case, the results of the parabolic approach are overall closer to the experiment.

The axial evolution of the centreline turbulent kinetic energy shown in fig.5b is calculated considering the configuration of Antoine et al. [5]. A good agreement was noted between the results of

the two codes in the different jet sections. By comparing the numerical results with those experimental of Antoine et al. [5], the results are in perfect agreement for $X \geq 50$.

So, we can conclude that the numerical results of the two codes obtained using the parabolic and elliptic approach are very close and practically similar. The comparison between the numerical and experimental data of Mesnier [4] and Antoine et al. [5] in the three jet areas, show a very acceptable and satisfactory agreement which validates the two calculations codes.

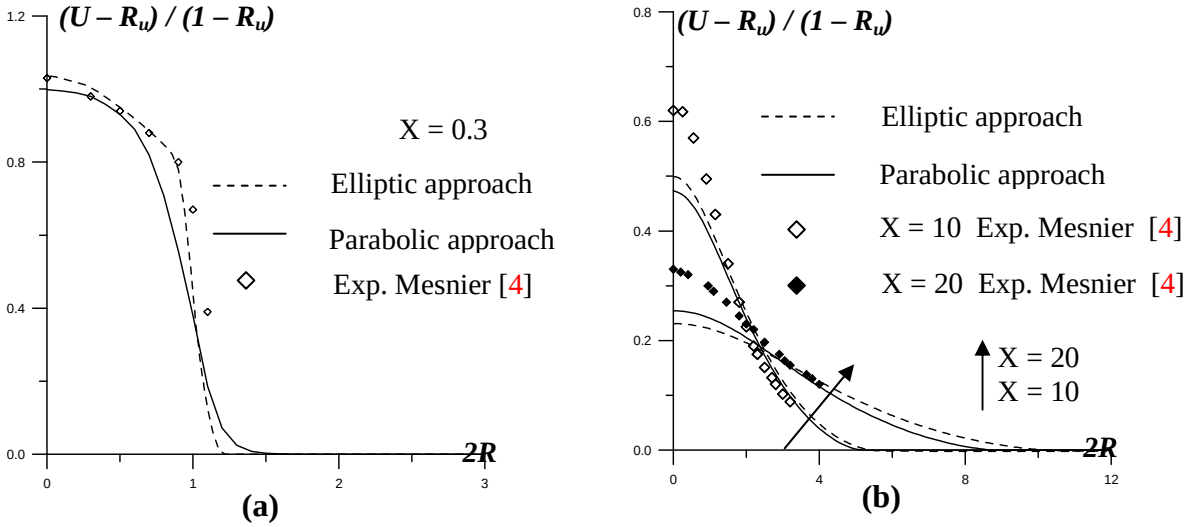

Fig.4. Radial evolution of the normalized vertical velocity

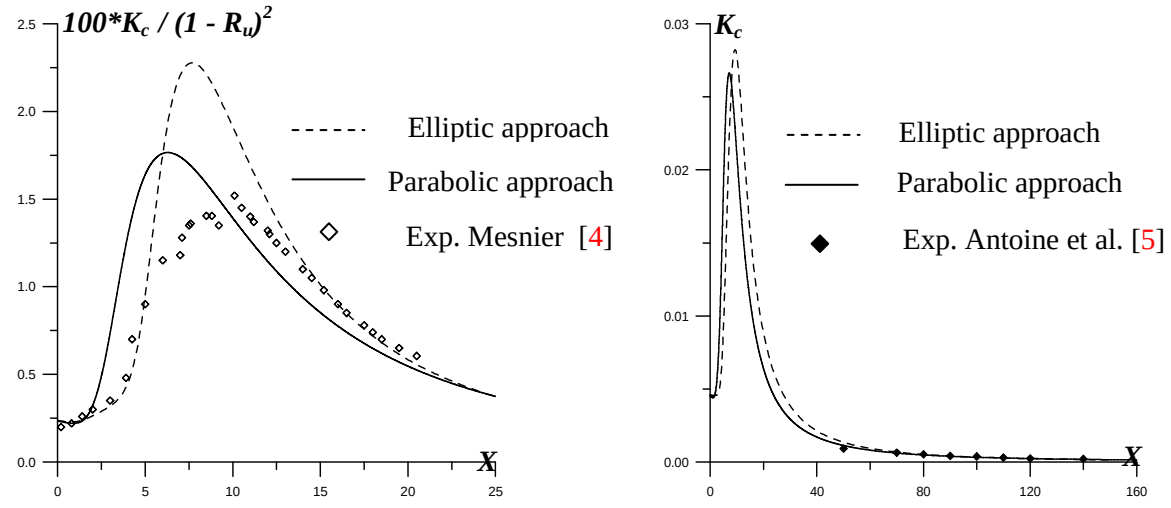

centerline turbulent kinetic energy **turbulent kinetic energy**

3.2. STUDY OF THE CO-FLOWING JET STRUCTURE USING THE PARABOLIC AND ELLIPTIC APPROACHES

In this section, we focus on the behavior of the co-flowing jet under a velocities ratios change by the aid of the parabolic and elliptic approaches. The calculations were carried out using the geometrical configuration of Mesnier [4] and the uniform emission profiles.

3.2.1. Study of the characteristic sizes of the flow

The comparison between the characteristic sizes of a co-flowing jet obtained by parabolic and elliptic approaches are investigated in this section, for different velocities ratios ranging between 0 and 10 and a Reynolds number Re equal to 23115. The main idea was to study the ability of the parabolic approach compared to the elliptic one to predict the co-flowing jet structure for all considered velocities ratios.

The axial evolution of the centerline vertical velocity U_c is given in fig.6 for different velocities ratios R_u. For $R_u \leq 1.5$ (Fig.6a), it is noted that the parabolic and elliptic approaches give similar results in the nozzle vicinity (initial zone of the jet). Nevertheless, the potential core length given by the elliptic approach is slightly greater than that of the parabolic approach. In the transition zone, whatever the value of R_u, a small difference which does not exceed 5% is observed between the results of the two approaches. In fact, more R_u moves away from 1 ($R_u \rightarrow 0$ or $R_u \rightarrow 1.5$), more this difference is remarkable but always lower than 5%. In the developed region, the two approaches give the same results. Thus, we can conclude that for velocities ratios $R_u \leq 1.5$, the two approaches give results practically similar and acceptable in the different jet regions, which confirms the validity of the parabolic approach. In fig.6b, we show the axial evolution of the centerline vertical velocity U_c for different velocities ratios R_u respectively equal to 2, 3.5 and 4.5. It is noted that the elliptic approach highlights in the nozzle vicinity an abrupt fall of the velocity which isn't visible by parabolic calculation. This fall takes values greater than zero and becomes more intense when R_u is larger. This phenomenon is ascribable with a non compensation of the momentum loss due to the trough of low pressure created by the secondary flow (co-flow) (Fig.7b). Further, in the established zone, the results of the two approaches become similar. Thus, we confirm that when R_u is greater than 1.5, the parabolic approach becomes inapt to predict the characteristic of the co-flowing jet especially the fall velocity marked by the elliptic approach. In fig.6c, we represent the evolution of U_c for different velocities ratios respectively equal to 5, 7 and 10. By comparing the results of the two approaches, we note that the elliptic approach shows an abrupt fall of the centerline vertical velocity to reach a minimal value U_{cmin} (appearance of the recirculation bubble), before growing for tending towards the co-flow velocity. This fall is more intense when R_u is larger. This recirculation zone that has not been detected by the parabolic approach is due to the use of the boundary layer approximations unable to describing the recirculation zone in the nozzle vicinity. So, for this flow regime, the parabolic approach is inapt to predict the structure of the jet discharged into a co-flow.

The axial evolutions of the centerline relative pressure determined by the parabolic and elliptic approaches for different velocities ratios R_u, are presented in fig.7. It is noted that for the parabolic approach P_c is almost constant and equal to zero for the different velocities ratios. For $R_u \leq 1.5$ (Fig. 7a), it is shown with the elliptic approach that the dimensionless centerline relative pressure is about 10^{-3} in the nozzle vicinity and tends towards zero for the great values of X. So, the pressure is very low and almost equal to zero in the all calculation field. In this case, the small depression detected in the nozzle vicinity does not have an effect on the vertical velocity (Fig.6a), which explains the absence of the fall velocity in this zone. For $1.5 < R_u < 5$ (Fig.7b), the centerline relative pressure takes important negative values in the nozzle vicinity (about 10^{-1}), from where appear the fall velocity (Fig.6b). In fact, as R_u increases as the depression becomes more important and the fall velocity intensifies in the nozzle vicinity. Just afterwards, the centerline pressure increases to reach a maximum which depends on R_u

and then tends towards zero downstream the nozzle. For $R_u \geq 5$ (Fig.7c), the depression detected in the nozzle vicinity becomes more intense and is at the origin of the velocity drop and hence the appearance of a recirculation bubble on the jet axis (Fig.7b).

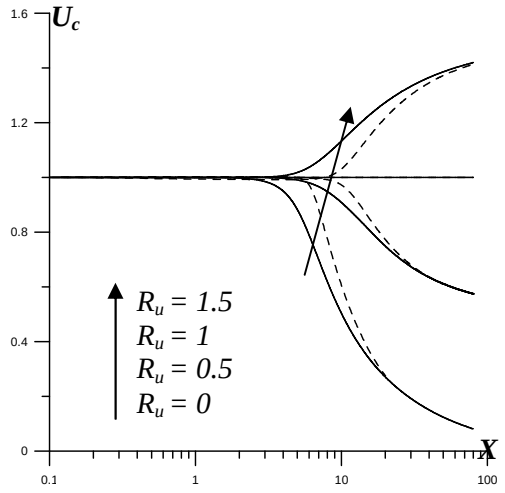

Fig.6a. $R_u \leq 1.5$

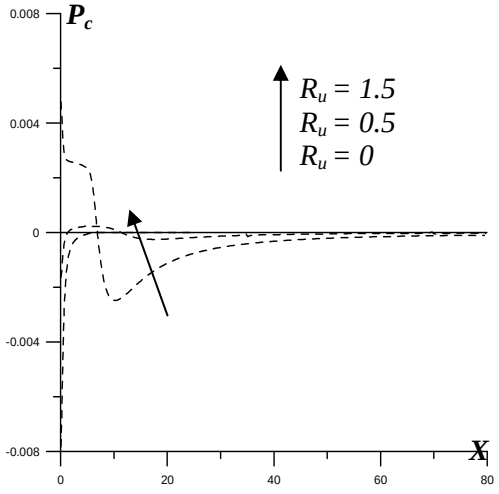

Fig.7a. $R_u \leq 1.5$

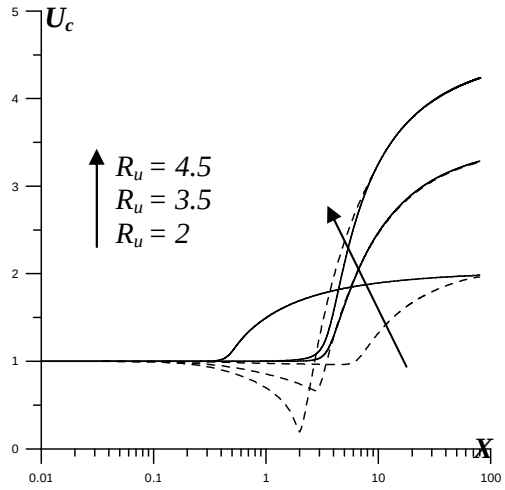

Fig.6b. $1.5 < R_u < 5$

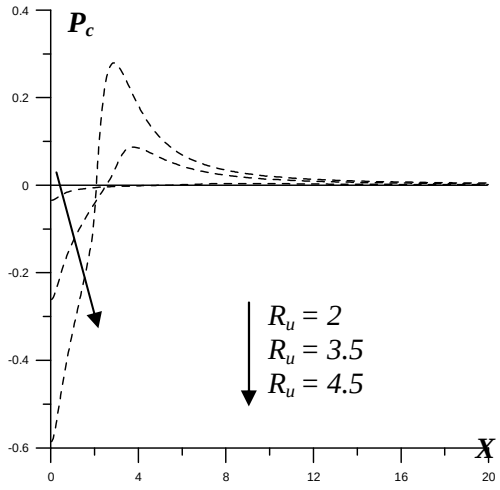

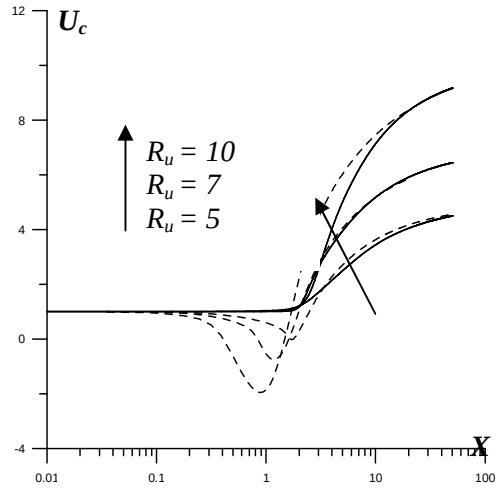

Fig.6c. $R_u \geq 5$

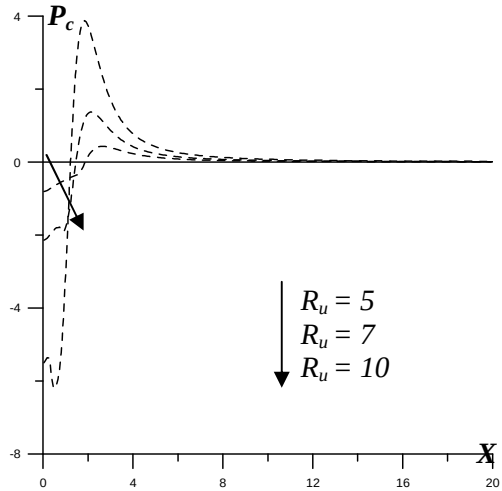

——— Parabolic approach ------ Elliptic approach

Fig.6. Axial evolution of the centerline vertical velocity

Fig.7. Axial evolution of the centerline relative pressure

3.2.2. Visualization of the turbulent co-flowing jet structure using the parabolic and elliptic approaches

To study the stream structure and the different flow regimes using the parabolic and elliptic approaches, the vertical velocity contours and the streamlines are presented in fig. 8, 9 and 10 for a broad range of velocities ratios R_u ranging between 0 and 10 (the jet velocity is taken constant and equal to 40 m/s) and a Reynolds number equal to 23115. From these figures, we can distinguish three cases: the first case where the depression is without any effect on the velocity (regime without recirculation bubble), $0 \leq R_u \leq 1.5$ (Fig.8). In the second case, the depression is with an effect on the velocity (regime without recirculation bubble), $1.5<R_u<5$ (Fig.9) and the third case where the depression is with recirculation bubble (regime with recirculation bubble), $R_u \geq 5$ (Fig.10).

The results of the parabolic and elliptic approaches were compared in fig.8, for three velocities ratios R_u respectively equal to 0, 0.5 and 1.5. We note that the two approaches give very close results and when R_u recedes from 1 *($R_u \rightarrow 0$ or $R_u \rightarrow 1.5$)*, the differences between the contours become noticeable but stay acceptable (Fig.6a). In this case *N°1* ($R_u \leq 1.5$), the boundary layer assumptions (parabolic approach) are considered valid, which is in agreement with the previous works who have adopted the parabolic approach to study the turbulent free jets [12] and the co-flowing jets [6-8] moving with low velocities ratios $R_u \leq 0.2$.

In fig.9, we compare the results of the parabolic and elliptic approaches for the velocities ratios R_u respectively equal to 2, 3.5 and 4.5. For the elliptic approach, it is noted the appearance of a noticeable fall velocity zone due to the presence of the trough low pressure (very important depression of about 10^{-1} in the nozzle vicinity (Fig.7b)). This drop that has not been seen by the parabolic approach is due to the phenomenon of the jet training by the outer stream. The intensity of this training is directly related to the difference between the primary (jet) and the secondary flow (co-flow). In fact, for the great velocities ratios, the sucked flux by the co-flow becomes more important and the fall velocity intensifies. Also, we note that when the fall velocity is important, the streamlines are very deformed. Thus, we conclude that the parabolic approach becomes unable to predict and to describe the structure of the co-flowing jet when R_u is greater than 1.5.

The flow regime with depression and recirculation bubble (case 3) is shown in fig.10 for the velocities ratios R_u respectively equal to 5, 7 and 10. The comparison between the results of the elliptic and parabolic approaches shows that when R_u increases, the elliptic approach highlights a recirculation zone which moves from the jet axis towards the outer nozzle edge. This recirculation zone that has not been detected by the parabolic approach is explained by the fact that the mass fluid provided by jet is not sufficient any more for the secondary flow when $R_u \geq R_{uc} = 5$, which creates a return of the downstream fluid. Thus, a negative vertical velocity zone is observed: this is the recirculation bubble. Moreover, the comparison between the streamlines of the two approaches shows that close to the nozzle, the elliptic approach streamlines are completely deformed compared to those of the parabolic approach. This character is due to the presence of recirculation zone. Thus, for this flow regime, the difference between the two approaches become obvious and the parabolic approach is inapt to describe the structure of the jet emerging in a co-flowing stream.

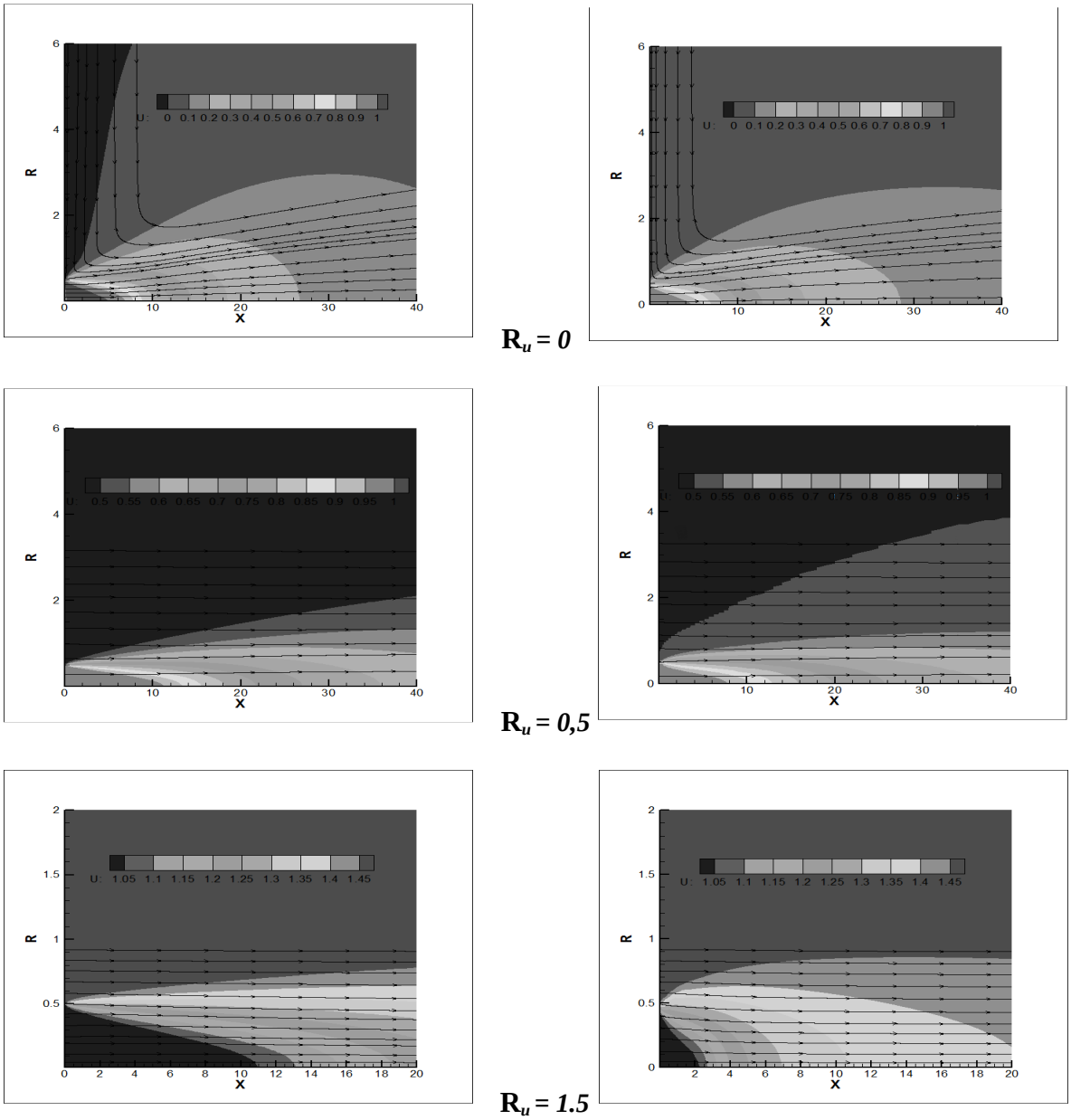

***Fig*.8. Vertical velocity contours and streamlines for the first case. (Depression without effect on velocity ($R_u \leq 1.5$))**

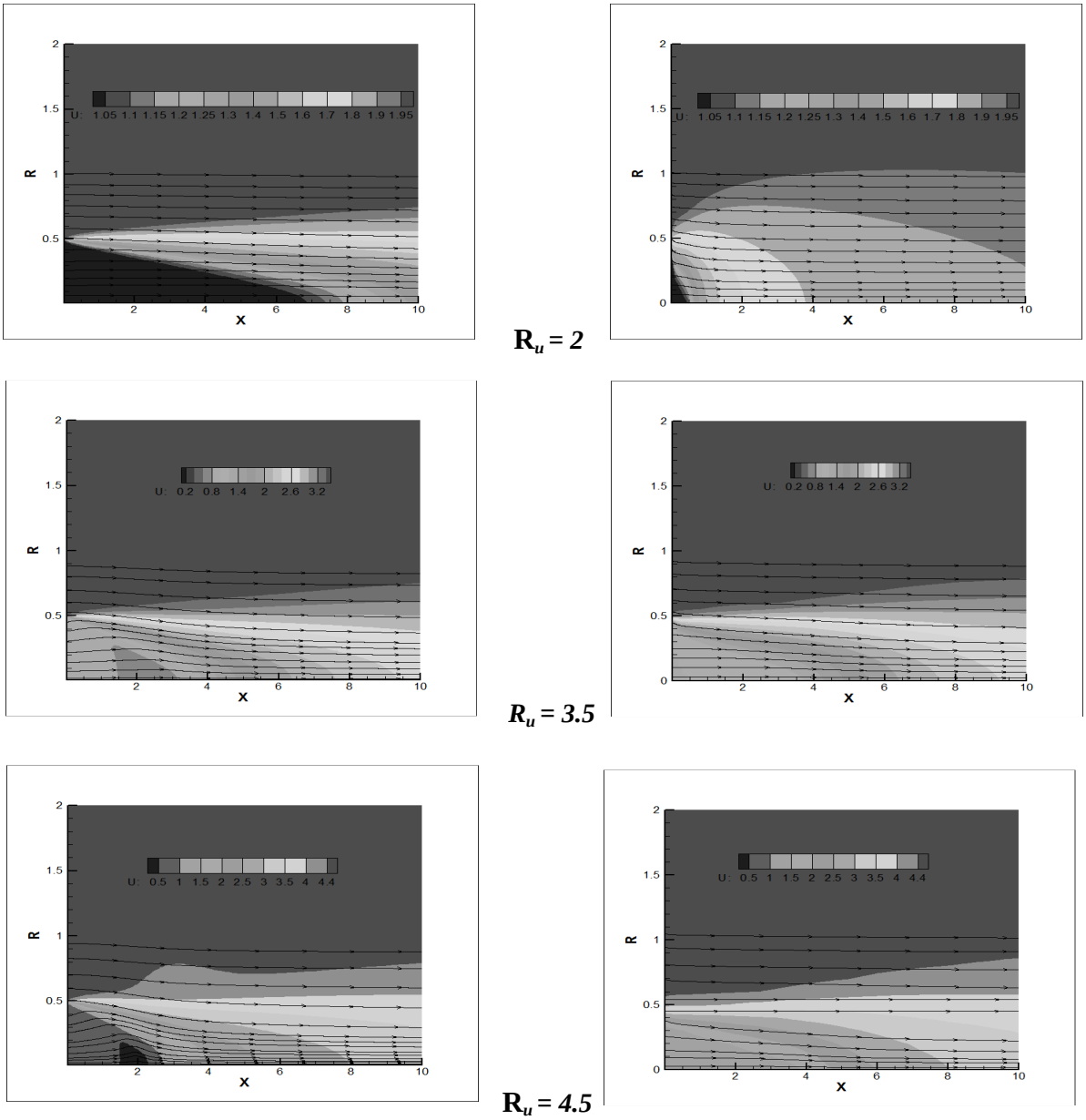

***Fig.*9. Vertical velocity contours and streamlines for the second case. (Depression with effect on velocity ($1.5< R_u <5$))**

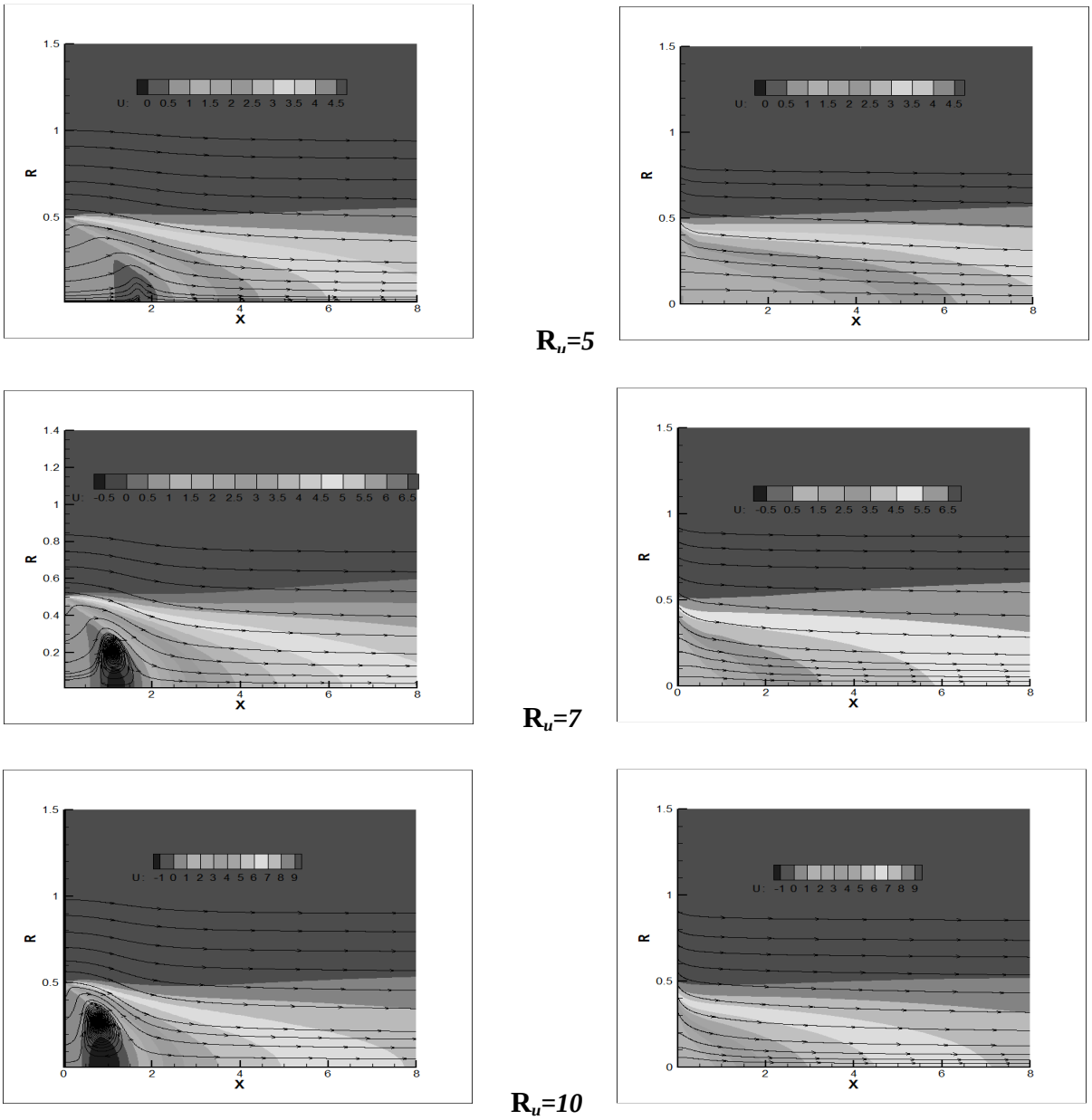

***Fig.*10. Vertical velocity contours and streamlines for the third case. (Depression with recirculation bubble ($R_u \geq 5$))**

4. Conclusion

In the present paper, a detailed comparison has been made for many statistical quantities, such as the axial evolution of mean streamwise velocity, turbulent kinetic energy, as well as radial profiles of vertical velocity. The agreement between simulation and experiment is generally very good for the elliptic and parabolic approaches. In the near filed, the numerical results deviate somewhat from the experimental data of Mesnier, presumably due to imperfection in the experiment.

According to the velocities ratio R_u, three cases and two flow regimes are identified: a depression produced without any effect on the velocity for $0 \leq R_u \leq 1.5$ (case1: regime without recirculation bubble). A drop pressure which is accompanied with an effect on the velocity for $1.5 < R_u < 5$ (Case 2: regime without recirculation bubble). Finally, the depression has an influence on the velocity and displays a recirculation bubble for $5 \leq R_u \leq 10$ (Case 3: regime with recirculation bubble). The origin of these two regimes is the entrainment between the jet and the ambient stream. The intensity of this phenomenon is related to the velocities difference. In fact, for the greatest velocities ratios, the sucked flux by the secondary stream becomes more important and the fall velocity intensifies. For $R_u \geq R_{uc} = 5$, this depression is sufficient to have a negative fall velocity and generate the recirculation bubble which migrates to the nozzle extremity according to the value of R_u.

The comparison between the results of the two approaches showed that the phenomena identified by the elliptic approach in both cases 2 and 3 are invisible by the parabolic approach. This concluded the validity of the parabolic approach compared to the elliptic one which is limited to the first case (depression without effect on the velocity) i.e. for $0 \leq R_u \leq 1.5$. In fact, for $R_u > 1.5$, the parabolic approach becomes unable to predict and to describe the structure and the characteristic parameters of the co-flowing jet.

Nomenclature

d nozzle diameter,[m]
k turbulent kinetic energy, [m^2s^2]
P static pressure, [Pa]
r transverse coordinates, [m]
Re Reynolds number, ($=ud/\nu$), [-]
R_u velocities ratio ($=u_\infty / u_0$), [-]
u, v mean velocity components along x and y directions, [m s^{-1}]
U, V dimensionless mean velocity components, [-]
U_{ex} excess velocity ($U_{ex} = U - U_\infty$), [-]
x longitudinal and coordinates, [m]

Greek symbols

ε dissipation rate of the turbulent kinetic energy, [m^2s^{-3}]
ν molecular kinematic viscosity, [m^2s^{-1}]
ν_t turbulent kinematic viscosity, [m^2s^{-1}]
ρ density, [$kg.m^{-3}$]

Subscripts

C jet axis
∞ ambient middle
0 nozzle exit

Superscript

$\bar{}$ Reynolds average

$'$ fluctuation

References

[1**]** Benarous, A., Liazid, A., H2-O2 supercritical combustion modeling using a CFD code, Thermal Science, 13 (2009), 3, pp. 139-152.

[2] Antonia, R. A., Bilger, R. W., An experimental investigation of an axisymmetric jet in a co-flowing air stream, Journal of fluid Mechanics, 61(1973), pp.805-822.

[3] Nickels, T. B., Perry, A. E., An experimental and Theoretical study of the turbulent coflowing jet, Journal Fluid Mechanics, 309(1995), pp. 157-182.

[4] Mesnier, B., Studies on the development of turbulent jets with variable density in axisymmetric and asymmetric geometries (In Frensh), Ph. D. Thesis, Orleans University, 2001.

[5] Antoine, Y., Fabrice, L., Michel, L., Turbulent transport of a passive scalar in a round jet discharging into a co-flowing stream, Journal Mechanics B. Fluids, 20**(**2001), pp. 275-301.

[6] Imine, B., et al., Study of non-reactive isothermal turbulent asymmetric jet with variable density, Comput. Mechanics, 38(2006), pp. 151–162.

[7] Habli, S., et al., Influence of a Coflowing Ambient Stream on a Turbulent Axisymmetric Buoyant Jet, Journal Heat Transfer, 130 (2008), 2, pp. 1-15.

[8] Wei-Biao, F., et al. The use of co-flowing jets with large velocity differences for the stabilization of low grade coal flames, Twenty first Symposium (International) on Combustion/the combustion Institute, 1986, pp. 567-574.

[9] Mahmoud, H., et al., A numerical study of a turbulent axisymmetric jet emerging in a co-flowing stream, Energy Conversion and Management, ELSEVIER, 51(2010), pp. 2117–2126.

[10] Martynenko, O. G., Korovkin, V. N., Flow and heat transfer in round vertical buoyant jets, International Journal Heat Mass Trans, 37(1994),1, pp.51-58.

[11] Hossain, M. S., Rodi, W., A turbulent model for boyant flows and its application to vertical boyant jets. Pergamon, New York, 1982, pp. 121–178.

[12] Habli, S., Mhiri, H., Golli, S., Etude numérique des conditions d'émission sur un écoulement de type jet axisymétrique turbulent, International Journal Thermal Science, 40(2001), pp. 497–511.

[13] Fluent Incorporated 6.2.16.